Hg Binding on Pd Binary Alloys and Overlays

Erdem Sasmaz, Shela Aboud, and Jennifer Wilcox*

Department of Energy Resources Engineering, School of Earth Sciences, Stanford University, Green Earth Sciences 065, 367 Panama Street, Stanford, California 94305

Received: December 19, 2008; Revised Manuscript Received: February 28, 2009

The vast majority of the mercury released from coal combustion is elemental mercury. Noble metals such as Pd, Au, Ag, and Cu have been proposed to capture elemental mercury. Density functional theory calculations are carried out to investigate mercury interactions with Pd binary alloys and overlays in addition to pure Pd, Au, Ag, and Cu surfaces using a projected augmented wave method with the Perdew−Wang generalized gradient approximation. It has been determined that Pd has the highest mercury binding energy in comparison to other noble metals. In addition, Pd is found to be the primary surface atom responsible for improving the interaction of mercury with the surface atoms in both Pd binary alloys and overlays. Deposition of Pd overlays on Au and Ag enhance the reactivity of the surface by shifting the d-states of surface atoms up in energy. Strong mercury binding causes a significant overlap between the s- and p-states of Pd and the d-state of mercury.

Introduction

Coal-fired power plants are the major source of mercury worldwide, and reducing the emissions of mercury is a major environmental concern since mercury is considered to be one of the most toxic metals found in the environment.[1] Additionally, Hg is reported as a hazardous air pollutant by the Clean Air Act (CAA) of 1990. Currently within the United States, there are more than five hundred 500-MW coal-fired power plants. The amount of energy produced from coal is predicted to increase 3% by 2030.[2] In 2005, the United States Environmental Protection Agency adopted the Clean Air Mercury Rule to reduce the release of Hg from coal-fired power plants by 70% in 2018.[3] In February 2008, this rule was vacated by the courts and power plants were removed from the CAA list of sources of hazardous air pollutants; however, roughly half of the states still have Hg emissions controls in place for coal-fired power utilities.

Depending on the coal type burned in boilers, oxidized and particulate forms of Hg can be captured in existing sulfur and particulate matter control devices as a cobenefit or by injecting sorbent materials such as chemically improved activated carbon into the flue gas stream. Recent investigations focused on the removal of elemental Hg in both pulverized coal-fired and integrated gasification combined cycle (IGCC) power plants. For IGCC power plants, Hg sorbents are required to withstand elevated temperatures. Noble metals such as Pd, Au, Ag, and Cu were proposed to adsorb Hg efficiently.[4−7] In particular, Pd sorbents showed enhanced Hg removal capacity at high temperatures.[4] There are numerous experimental[4,5,8−15] and theoretical[6,7,16] studies for Hg adsorption on metal surfaces. Additionally, many studies indicate a higher reactivity of Pd overlays on noble metals with different kinds of adsorbates.[17−24] An important issue with implementing Pd sorbents in flue and fuel gas environments is dealing with sulfur poisoning. Although the trend is weakly pronounced, previous studies indicated weak binding behavior of sulfur on Pd binary alloys.[25] Therefore, these Pd binary alloys are investigated in the current study to test their Hg reactivity. The major purpose of this work is to determine the binding mechanism of Hg on noble metals, Pd binary alloys, and overlays and to understand their surface reactivity by examining their electronic structure. In this manner, DFT calculations were carried out to examine Hg binding on Pd(111), M(111) (M = Au, Ag, Cu), Pd−M(111) binary alloys, and Pd/M(111) overlays.

Computational Methodology

DFT calculations were performed with the Vienna ab initio simulation package.[26−28] Core orbitals were described using the projected augmented wave method,[29,30] and exchange-correlation energies were calculated with the Perdew−Wang (PW91)[31,32] generalized gradient approximation (GGA). A plane-wave expansion with a cutoff of 350 eV was found to be sufficient in all the calculations to obtain the converged results. Gaussian-smearing of order one was used with a width of 0.05 eV, maintaining a difference of 1 meV/atom between the calculated free energy and total energy. For bulk materials, equilibrium lattice constants and cohesive energies were calculated and are presented in Table 1. The lattice constants were found to be overestimated with GGA with a relative error of less than 2.2% in comparison to experimental measurements. In addition, a comparison of cohesive energies and corresponding experimental measurements indicates that GGA underestimates the cohesive energies of bulk metals and alloys by a relative error of 3−20%.[33,34]

The binding of Hg on (111) surfaces of Pd, M, Pd/M overlays, and Pd−M alloys was investigated using 4−7 layer slabs separated with at least a 12 Å vacuum region. The two bottom layers of each slab were fixed at the bulk geometry, while the upper layers including the overlays and Hg were allowed to relax. Geometric relaxation was obtained with the conjugate-gradient algorithm until the forces on all the unconstrained atoms were less than 0.01 eV/Å. All the calculations were carried out on p(2 × 2) surfaces with four metal atoms per layer, as shown in Figure 1a, and the surface Brillouin zone integration was calculated with a 7 × 7 × 1 Monkhorst−Pack[35] *k*-point mesh. To test the convergence of the slab calculations, binding

* To whom correspondence should be addressed. Tel.: 650-724-9449. Fax: 650-725-2099. E-mail: wilcoxj@stanford.edu.

10.1021/jp8112478 CCC: $40.75
Published on Web 04/14/2009

TABLE 1: Lattice Constant and Cohesive Energies of Bulk Materials

	calcd		exptl	
	lattice constant (Å)	cohesive energy (eV)	lattice constant[a] (Å)	cohesive energy[b] (eV)
Pd	3.96	3.77	3.89	3.89
Au	4.17	3.05	4.08	3.81
Ag	4.16	2.55	4.09	2.95
Cu	3.64	3.53	3.62	3.49
Pd_3Ag	4.00	3.49	3.92	3.65
Pd_3Au	4.01	3.62	3.94	3.87
Pd_3Cu	3.89	3.77	3.82	3.79
$PdAg_3$	4.10	2.91	4.02	3.18
$PdAu_3$	4.12	3.29	4.03	3.83
$PdCu_3$	3.74	3.66	3.70	3.59

[a] Reference 33. [b] Elements: Reference 34; Alloys: Reference 34, where data for alloys is calculated.

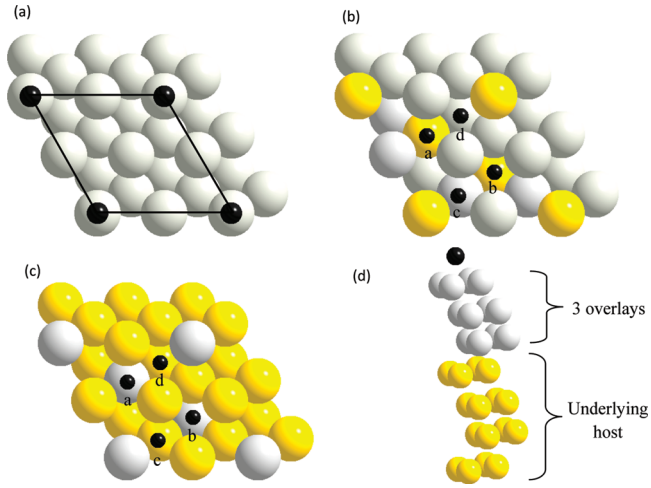

Figure 1. (a) Scheme of a p(2 × 2) supercell of (111) surfaces. (b) Threefold adsorption sites of Pd_3M binary alloys: a. pure-hcp site, b. pure-fcc site, c. mixed-hcp site, d. mixed-fcc site. (c) Threefold adsorption sites of PdM_3 binary alloys: a. pure-hcp site, b. pure-fcc site, c. mixed-hcp site, d. mixed-fcc site. (d) Side view of 3Pd/M(111) structure.

energies, work functions, and d-band centers of the Pd(111) + Hg system were examined as a function of *k*-point mesh size and number of slab layers. It was found that the binding energies, work functions, and d-band centers differ by 0.002, 0.023, and 0.04 eV, respectively, in comparison to a 9 × 9 × 1 *k*-point mesh and a seven-layer slab. To represent the Hg-adsorbed structure, a single adatom was placed on the surface corresponding to a coverage of $\theta = 0.25$ ML. The Pd overlays were modeled with up to three Pd overlays, and the surface composition of the Pd monolayer was varied in the case of one Pd overlay. Different compositions of Pd−M alloys were modeled in our group previously.[7] However, to investigate the effect of Hg binding, the specific alloy compositions $Pd_3M(111)$ and $PdM_3(111)$ were studied in the current work in greater detail. The alloy surfaces were modeled as ordered fcc structures where the top layer composition has the same stoichiometry as the bulk. Although in practice these alloys often exist as disordered systems,[36−40] only ordered surfaces were examined in this work to gain a fundamental understanding of the interaction between Hg and the different metal atoms in the alloys and how this interaction changes as a function of neighboring atoms. Further discussion about ordered and disordered alloys should be read in the Results and Discussion section.

TABLE 2: Binding Energies of Hg on High Symmetry Adsorption Sides

	E_{bind} (eV)			
	Pd(111)	Au(111)	Ag(111)	Cu(111)
bridge		−0.32	−0.35	−0.52
hcp	−0.84	−0.34	−0.37	−0.54
fcc	−0.84	−0.35	−0.38	−0.55
top		−0.28	−0.28	−0.42

The binding energy of Hg, E_{bind}, at each surface site was calculated using eq 1:

$$E_{bind} = E_{slab+Hg} - [E_{Hg} + E_{slab}] \quad (1)$$

where $E_{slab+Hg}$, E_{Hg}, and E_{slab} represent the total energies of the relaxed substrate plus Hg, the adsorbate Hg atom, and the substrate surface, respectively. Subsequently, a more negative binding energy represents a stronger interaction. Wigner and Bardeen[41] defined the work function as the difference between the energy necessary for the electrons to pass through the dipole barrier at the surface and the bulk chemical potential with respect to the metal interior. The work function, ϕ, is equivalent to the minimum energy required to extract one electron from inside the bulk to an infinite distance. Here, the work function of the clean and Hg-bound surfaces is calculated as $\phi = V_0 - E_F$, where V_0 is the energy level in the vacuum region defined sufficiently far from the surface and E_F is the Fermi energy.[42] The corresponding change in charge density giving rise to the surface dipole is also examined and is calculated with eq 2, where the $x-z$ plane lies parallel and perpendicular to the surface:

$$\Delta\rho(x,z) = \rho_{tot}(x,z) - \rho_{surf}(x,z) - \rho_{ads}(x,z) \quad (2)$$

where the first term is the total charge density, the second term is the charge density of the bare surface, and the third term is the charge density of the Hg adsorbate atom.

Results and Discussion

Binding Energy. The interaction between Hg and pure Pd(111), Au(111), Ag(111), and Cu(111) surfaces on hollow, bridge, and top adsorption sites was investigated using p(2 × 2) supercells with calculated binding energies compared against experimental measurements as reported in Table 2. The strongest binding occurred at both fcc and hcp hollow sites on all metal surfaces, whereas weaker binding took place on bridge and top adsorption sites. The difference in the binding energies on hcp and fcc hollow sites is found to be negligible. For the Pd(111) surface, no stable geometry was found on bridge or top

TABLE 3: Hg Adsorption on hcp Sites of (111) Metal Surfaces, and Overlays and fcc, hcp, mhcp, and mfcc Sites of $Pd_3M(111)$ and $PdM_3(111)$ Binary Alloys[a]

	E_{bind} (eV)	Pd−Hg (Å)	M−Hg (Å)	Φ (eV)	ΔΦ (eV)	ε_d (eV)	ε_d' (eV)
Pd(111)	−0.84	2.84		5.31	−1.04	−1.83	−2.18
Au(111)	−0.34		3.02	5.21	−0.91	−3.39	−3.71
Ag(111)	−0.37		3.01	4.47	−0.52	−4.07	−4.25
Cu(111)	−0.54		2.77	4.75	−0.88	−2.52	−2.77
Pd_3M Alloys							
$Pd_3Ag(111)$-fcc	−0.79	2.82	3.92	5.18	−0.97	−2.18	−2.38
$Pd_3Ag(111)$-hcp	−0.88	2.82	3.91	5.18	−0.99	−2.18	−2.38
$Pd_3Ag(111)$-mfcc							
$Pd_3Ag(111)$-mhcp	−0.72	2.79	3.07	5.18	−1.00	−2.18	−2.38
$Pd_3Au(111)$-fcc	−0.84	2.81	3.95	5.37	−1.21	−2.04	−2.38
$Pd_3Au(111)$-hcp	−0.87	2.84	4.58	5.37	−1.13	−2.04	−2.38
$Pd_3Au(111)$-mfcc							
$Pd_3Au(111)$-mhcp	−0.76	2.78	3.07	5.37	−1.19	−2.04	−2.38
$Pd_3Cu(111)$-fcc	−0.72	2.84	4.01	5.15	−0.89	−1.83	−2.18
$Pd_3Cu(111)$-hcp	−0.83	2.84	4.01	5.15	−0.98	−1.83	−2.18
$Pd_3Cu(111)$-mfcc	−0.78	2.83	2.71	5.15	−1.04	−1.83	−2.18
$Pd_3Cu(111)$-mhcp	−0.76	2.85	2.67	5.15	−1.02	−1.83	−2.18
PdM_3 Alloys							
$PdAg_3(111)$-fcc	−0.41	4.99	2.89	5.15	−0.82	−3.29	−3.33
$PdAg_3(111)$-hcp	−0.36	4.93	3.04	5.15	−0.48	−3.29	−3.33
$PdAg_3(111)$-mfcc	−0.63	2.72	3.11	5.15	−0.75	−3.29	−3.33
$PdAg_3(111)$-mhcp	−0.65	2.73	3.06	5.15	−0.78	−3.29	−3.33
$PdAu_3(111)$-fcc	−0.46	4.17	2.94	4.73	−1.23	−2.83	−3.11
$PdAu_3(111)$-hcp	−0.36	4.25	3.03	4.73	−0.67	−2.83	−3.11
$PdAu_3(111)$-mfcc	−0.61	2.74	3.06	4.73	−1.09	−2.83	−3.11
$PdAu_3(111)$-mhcp	−0.63	2.75	3.01	4.73	−1.14	−2.83	−3.11
$PdCu_3(111)$-fcc	−0.53	3.78	2.75	4.89	−1.00	−2.19	−2.46
$PdCu_3(111)$-hcp	−0.49	2.81	3.81	4.89	−0.54	−2.19	−2.46
$PdCu_3(111)$-mfcc	−0.60	2.78	2.86	4.89	−0.86	−2.19	−2.46
$PdCu_3(111)$-mhcp	−0.63	2.79	2.81	4.89	−0.97	−2.19	−2.46
Pd Overlays							
PdM_3/Au(111)	−0.42	4.28	2.99	5.25	−0.84	−2.74	−3.65
PdM_3/Ag(111)	−0.38	4.29	3.02	4.61	−0.48	−3.36	−4.20
PdM_3/Cu(111)	−0.50	3.74	2.81	4.90	−0.82	−2.45	−2.73
PdM/Au(111)	−0.56	2.76	3.06	5.27	−1.01	−2.39	−3.62
PdM/Ag(111)	−0.54	2.77	3.11	5.55	−0.65	−2.64	−4.05
PdM/Cu(111)	−0.50	2.88	2.87	5.06	−0.88	−2.25	−2.61
Pd_3M/Au(111)	−0.93	2.81	4.01	5.29	−0.98	−1.90	−3.57
Pd_3M/Ag(111)	−0.92	2.81	3.99	5.32	−0.80	−1.84	−3.88
Pd_3M/Cu(111)	−0.56	2.88	2.97	5.34	−1.07	−2.26	−2.53
Pd/Au(111)	−0.93	2.81	4.47	5.22	−0.89	−1.49	−3.52
Pd/Ag(111)	−0.91	2.81	4.46	5.58	−0.98	−1.30	−3.84
Pd/Cu(111)	−0.58	2.96	4.76	5.51	−1.05	−2.37	−2.45
2Pd/Au(111)	−1.03	2.78	6.83	5.30	−1.08	−1.52	−1.86
2Pd/Ag(111)	−1.05	2.73	6.86	5.55	−1.12	−1.43	−1.87
3Pd/Au(111)	−0.96	2.79	8.96	5.19	−0.98	−1.62	−2.04
3Pd/Ag(111)	−0.96	2.79	9.01	5.47	−1.00	−1.53	−2.02

[a] E_{bind} denotes binding energy of Hg; Pd−Hg and Pd−M denote distances between atoms; Φ denotes work function of clean metal surfaces; ΔΦ denotes work function change after Hg adsorption; ε_d denotes weighted d-band center of clean surfaces; and ε_d' denotes weighted d-band center of subsurfaces.

adsorption sites. The binding energies of Hg on four noble metals occur in the following order: $E_{bind}(Pd) > E_{bind}(Cu) > E_{bind}(Ag) > E_{bind}(Au)$.

Hg binding on $Pd_3M(111)$ and $PdM_3(111)$ binary alloys was calculated for the hollow, bridge, and top adsorption sites. Because of the binary composition on the surface, additional hollow, bridge, and top adsorption sites were also present. However, the bridge and top adsorption sites are again found to be less stable in comparison to the hollow sites, and thus the Hg binding energy is only presented for the mixed and pure hollow adsorption sites, as shown in Figure 1b,c. The binding energies presented in Table 3 indicate that stronger Hg binding can be obtained on pure-hcp sites of $Pd_3Ag(111)$ and $Pd_3Au(111)$ surfaces compared to those of Pd(111), Ag(111), Au(111), and Cu(111) surfaces. Further increase (beyond 25% composition) of the percentage of Au, Ag, and Cu in Pd binary alloys causes Hg binding to weaken. Additionally, Hg is found to interact weakly with mixed fcc and hcp sites compared with pure sites on the Pd_3M (111) surfaces, whereas the opposite is true on the $PdM_3(111)$ surfaces. In particular, Hg prefers to remain on pure-hcp sites of $Pd_3Ag(111)$ and $Pd_3Au(111)$ surfaces and no stable geometry was found at the corresponding mixed fcc sites. The bond distances between Hg and the nearest substrate atoms, reported in Table 3, suggest that stronger Hg binding can generally be obtained when Hg is closer to the surface Pd atoms rather than the surface M atoms. The addition of 25% Ag or Au in Pd (Pd_3M) binary alloys can either improve Hg binding or decrease the binding energy of Hg depending

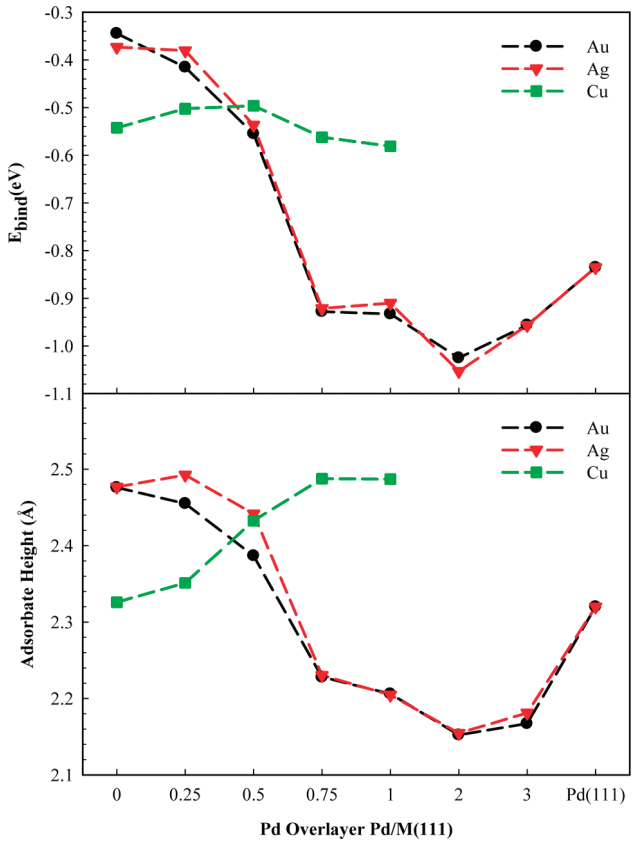

Figure 2. Binding energy and adsorbate height of Hg on Pd/M(111) overlays. Numbers smaller than 1 in the *x*-axis represent the surface composition of Pd in one Pd overlay.

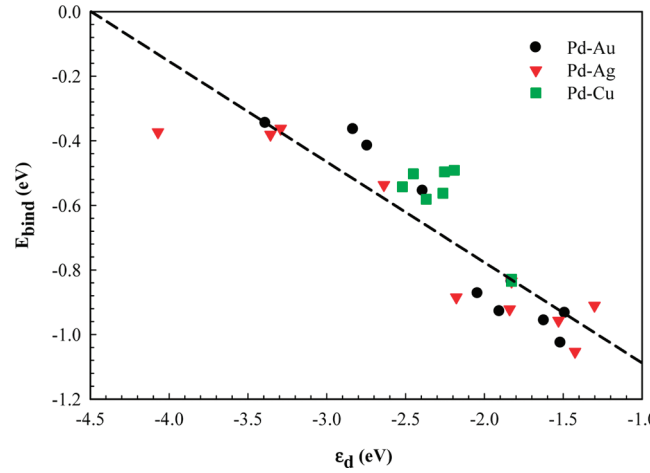

Figure 3. Center of d-band of surface atoms of Pd binary alloys and overlays as a function of Hg binding energy.

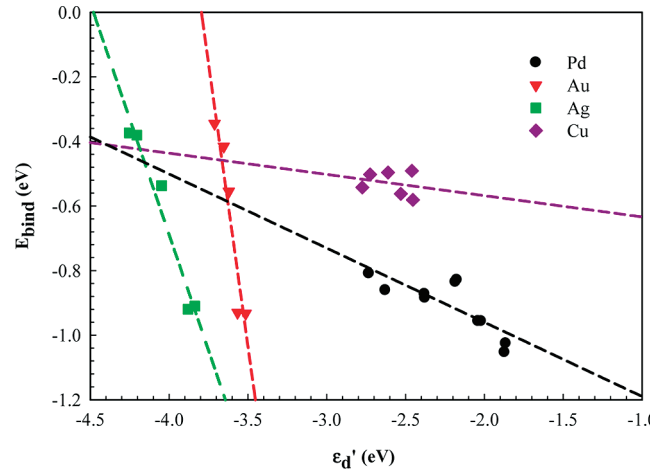

Figure 4. Center of d-band of subsurface atoms of Pd binary alloys and overlays as a function of Hg binding energy.

on the adsorption site. This behavior demonstrates the sensitivity of Hg binding to the position of the Pd and M atoms surrounding the adsorption sites. Specifically, M atoms improve the Hg reactivity of surface Pd atoms when they are located in subsurface layers of the alloy, as reported in previous work.[7] It is important to note that throughout the alloy calculations, the binding energy of Hg is calculated on highly ordered p(2 × 2) surfaces. In real systems, Pd and M atoms can form disordered alloys and the randomness of the position of the atoms can affect Hg binding on the surface. Simulating disordered alloys is computationally expensive because of the larger super cell size required and increased number of permutations by which an adsorbate can bind. However, it is important to gain insight into the fundamental mechanisms that can enhance or reduce the binding strength from the ordered alloy investigations to estimate the binding energy of Hg on the more realistic disordered alloy surfaces. For ordered Pd_3M alloys, stronger and weaker binding occurs at the hollow sites that are formed with 3Pd (pure site referring to 3 Pd atoms surrounding an adsorbent site) and 2Pd (mixed site) atoms, respectively. Since different orientations exist on disordered Pd_3M alloys, additional hollow sites can be formed with 1Pd or 3M atoms. Therefore, weaker Hg binding can be found on these sites in comparison to the 2Pd hollow sites that exist in the ordered Pd_3M alloys.[7] However, the strongest binding is still observed on the 3Pd hollow sites. Although weaker Hg binding will probably be obtained on disordered Pd_3M alloys, the probability of finding 1Pd and 3M hollow sites on the surface is low and thus the binding energy of Hg on disordered and ordered alloys in this case is expected to be similar. In the case of the disordered PdM_3 alloys, the same analogy can be made. Accordingly, 2Pd and 3Pd hollow sites will yield stronger Hg binding, but the weakest binding will still be on 3M hollow sites.

One concern when using these metal surfaces under realistic environmental conditions is that the surface can be poisoned by sulfur, leading to a subsequent decrease in Hg adsorption. Previously, Alfonso et al. studied the interaction of S with noble metals and PdAg and PdCu binary alloys[25] and found that sulfur binds strongly at the threefold adsorption sites and a weak trend was observed in the reduction of the sulfur binding energy on the alloy surfaces compared to the same sites on the Pd(111) surface. In particular, the binding energy of sulfur was found to be lower on pure hollow sites of $PdCu_3$ and $PdAg_3$ alloys, which is a trend also observed for Hg in the current work. A comparison between S and Hg binding on Pd binary alloys clearly indicates that both adsorbates are attracted to the same surface atoms and bind to the same adsorption sites. Since the concentration of sulfur compared to Hg is higher in both flue and fuel gas environment, it is expected that sulfur poisoning will occur on the surface. Further studies are required to design a surface that will effectively minimize sulfur poisoning while enhancing Hg binding.

The binding of Hg on Pd_3M and PdM_3 binary alloys shows that the capacity of Pd atoms to adsorb Hg can be enhanced when the dopant M atoms in the alloy are located in subsurface layers. The next step is to examine Hg adsorption on overlays of Pd on M(111) surfaces. It has been well documented that

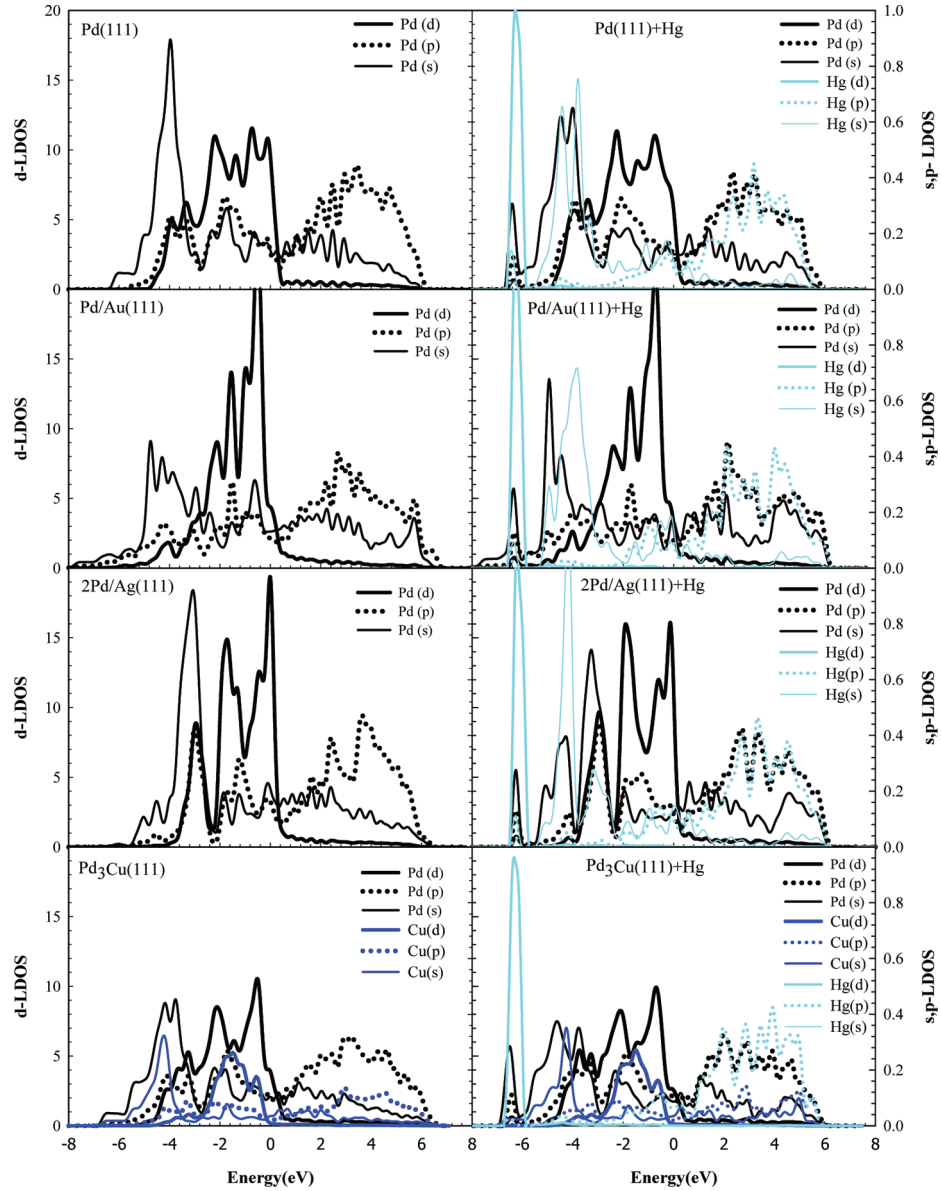

Figure 5. L-DOS graphs of metal atoms in Pd(111) + Hg, Pd/Au(111) + Hg, 2Pd/Ag(111) + Hg, and $Pd_3Cu(111)$ + Hg structures before and after Hg binding.

strained metallic overlays can improve the surface reactivity.[21,22,43−45] In addition, for Pd/Au(111) and Pd/Cu(111) overlays it is possible to observe layer-by-layer growth with up to four Pd overlays on Au(111) under electrochemical conditions.[46−50] However, more recent studies indicate that perfect layer-by-layer growth of Pd on Cu(111) does not occur because of the lattice mismatch (7.45%) between the Pd and Cu crystals. This work also reported that, after approximately two overlays, the lattice spacing of Pd reaches the value of pure Pd(111).[51,52] Furthermore, Christensen et al. calculated the segregation energy of Pd on Au, Ag, and Cu host atoms, which were found to be −0.14, −0.3, and 0.13 eV/atom, respectively.[53] The segregation energy of one Pd atom on a surface of host atoms of type M shows that Pd atoms are expected to remain on the surface layer of Au(111) and Ag(111) and migrate to subsurface layers in Cu(111). In the current study, Pd overlays were investigated with up to three overlays on Au(111) and Ag(111) surfaces, as shown in Figure 1d, and the surface composition of a single Pd overlay was varied between 25 and 100% Pd. For the Pd/Cu(111) overlays, Hg binding was only examined on one Pd overlay on Cu(111) because of the complex growth mechanism of Pd on Cu.[51] Binding energies and adsorption height of Hg on Pd/M(111) overlays were only calculated at hcp sites and are summarized in Figure 2. In all of the overlay cases studied, Pd overlay substrates appear to increase the binding energy of Hg in comparison to the M(111) surfaces. In particular, in Pd/Au(111) and Pd/Ag(111) overlay structures, stronger Hg binding occurs compared to those of the pure Pd(111) surfaces. In both cases, the binding energies of Hg are up to 0.1−0.2 eV larger than the pure Pd(111) surface and reach a maximum value on the surfaces with two Pd overlays. This is also consistent with the adsorbate height which reaches the lowest value in the two Pd/Au(111) and Pd/Ag(111) overlays. For the Pd/Cu(111) overlays, the binding energy of Hg fluctuates slightly with increasing Pd surface composition and the adsorbate height shows a 0.16 Å increase. The reason for an increase in the adsorbate height might be due to the Cu host atoms reducing the reactivity of the Pd overlays because of the larger distance between the Hg and the surface compared to that of the pure Pd(111) surface. Again, bond distances between Hg and the nearest Pd atom, as presented in Table 3, on Pd/M(111) overlays are found to be closer in the cases of

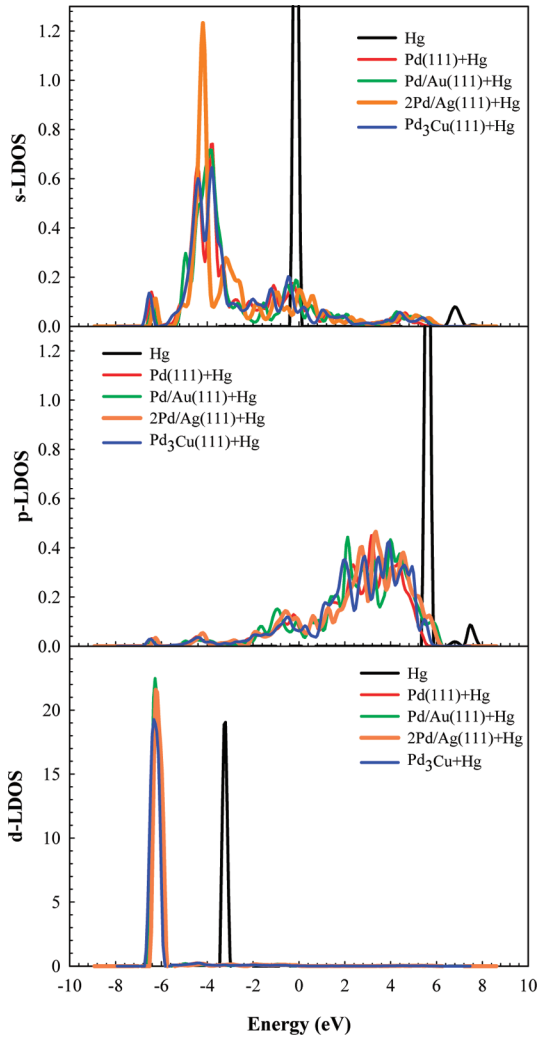

Figure 6. L-DOS graphs of Hg in Pd(111) + Hg, Pd/Au(111) + Hg, 2Pd/Ag(111) + Hg, and $Pd_3Cu(111)$ + Hg structures before and after Hg binding.

strong Hg binding. Larger binding energies on the Pd/Au(111) and Pd/Ag(111) overlays are the result of the lattice expansion of Pd substrates (strain effect) and the subsequent electronic effect of the underlying host. The lattice constant of Au and Ag is ~5% larger than the lattice constant of Pd, which leads to a lattice expansion of Pd overlays by ~5%. As the number of Pd overlays increases on Au and Ag, the bulk properties of Pd will start to be observed and the electronic effect of the underlying host will be suppressed. At this point, the reactivity of Pd overlays will be strongly dominated by the strain effects. The strain effect of the underlying host on the binding energies of Hg can also be seen on Pd/Cu(111) overlays. Since Cu has a smaller lattice constant than Pd, a decrease of the lattice constant of Pd overlays is expected, which yields a weaker Hg binding compared to the case of the pure Pd(111) surface. To further understand the interaction of Pd overlays on Au, Ag, and Cu metals, the binding energy of one Pd atom was calculated on p(2 × 2) cells of M(111) surfaces and compared with that of the pure Pd(111) surface. It was observed that one Pd atom is bound weakly to Au(111) (0.07 eV) and Ag(111) (0.18 eV) surfaces and bound more strongly to the Cu(111) (−0.27 eV) surface in comparison to the pure Pd(111) surface. Compared to the Pd(111) surface, the bond distances of Pd with the surface atoms are found to be longer on Au(111) and Ag(111) surfaces and shorter on the Cu(111) surface. Weak binding of Pd on Au and Ag indicates that Pd has less of an overlap with the underlying host material, which leads to a stronger surface−adsorbate interaction. Similar behavior is also reported by other authors where they studied the reactivity of Pd overlays on Au.[21,22] Strong Hg interactions on both 2Pd/Au(111) and 2Pd/Ag(111) overlays demonstrate the effect of the subsurface layer on Hg binding, where 2Pd/M(111) denotes two monolayers of Pd on a Au(111) surface. Although the surface composition is exactly the same in both the one- and two-Pd overlays, the difference of the subsurface composition yields the higher reactivity. The effect of the subsurface layer is also observed at the fcc and hcp sites of Pd_3M and PdM_3 alloys. The different binding energies calculated at the fcc and hcp sites are the result of the composition of the second nearest neighbors in the subsurface layer.

Electronic Structure. Nørskov and co-workers previously showed that the strength of the binding energy of an adsorbate on a transition-metal surface is related to the coupling between adsorbate energy levels and transition-metal d-bands.[45,54−62] The reactivity of a transition metal depends on the position of the d-band center relative to the Fermi level, d-bandwidth, and the occupancy of the d-bands. As the d-bandwidth gets narrower, the density of states around the Fermi level enlarges and the magnitude of the coupling matrix element decreases, thereby increasing the reactivity of the metal.[45,58] Among the three factors listed, the energy of the d-band center is the leading factor since it determines the energy position of the adsorbate metal bonding and antibonding states.[63] The d-band center for the surface (ε_d) and subsurface (ε_d') metal atoms was calculated by taking the first moment of the normalized projected density of states up to the Fermi level[57] as presented in Table 3. Figure 3 shows the d-band center of the surface atoms in Pd(111), M(111), $PdM_3(111)$, $Pd_3M(111)$, and Pd/M(111) structures as a function of Hg binding energy. It is clear that there is a fairly linear relation between the d-band center of the surface atoms and Hg binding. Because the total number of electrons is conserved in the adsorbate−substrate interaction, the lattice expansion of the Pd atoms reduces the d-bandwidth, leading to an upshift of the d-band center.[59] The effect of the substrate atoms, located in the subsurface layers, on the binding of Hg was mentioned previously. It was found that when like atoms are grouped together, the d-band center of subsurface atoms also exhibits a linear relationship with Hg binding energy, as shown in Figure 4. Grouping the same atoms together minimizes the effect of the coupling matrix element, resulting in an enhanced linear relationship. As observed in the case of surface atoms, the d-band center of subsurface atoms shifts down with smaller Hg binding energies.

The change in work function of all (111) surfaces after Hg binding stems from charge reorganization, which affects the surface dipole moment in addition to the Smoluchowski smoothing.[42] A decrease in the work function after binding is the consequence of a positive dipole layer, which leads to a charge transfer from the adsorbate to the substrate. In all surfaces, the adsorbate-induced work function decreases after Hg binding, as shown in Table 3. A decrease in the adsorbate-induced work function indicates the electropositive behavior of Hg, which is consistent with the previous work of Steckel.[6] To understand the impact of Hg on Pd alloys and overlays, the local density of states (L-DOS) of surface atoms was examined. Overall, the L-DOS corresponding to the different surfaces with the stronger Hg interactions, such as Pd/Au(111), 2Pd/Ag(111), and $Pd_3Cu(111)$, is studied and compared with pure Pd(111). As shown in Figure 5, the d-bandwidth of Pd on the clean Pd/

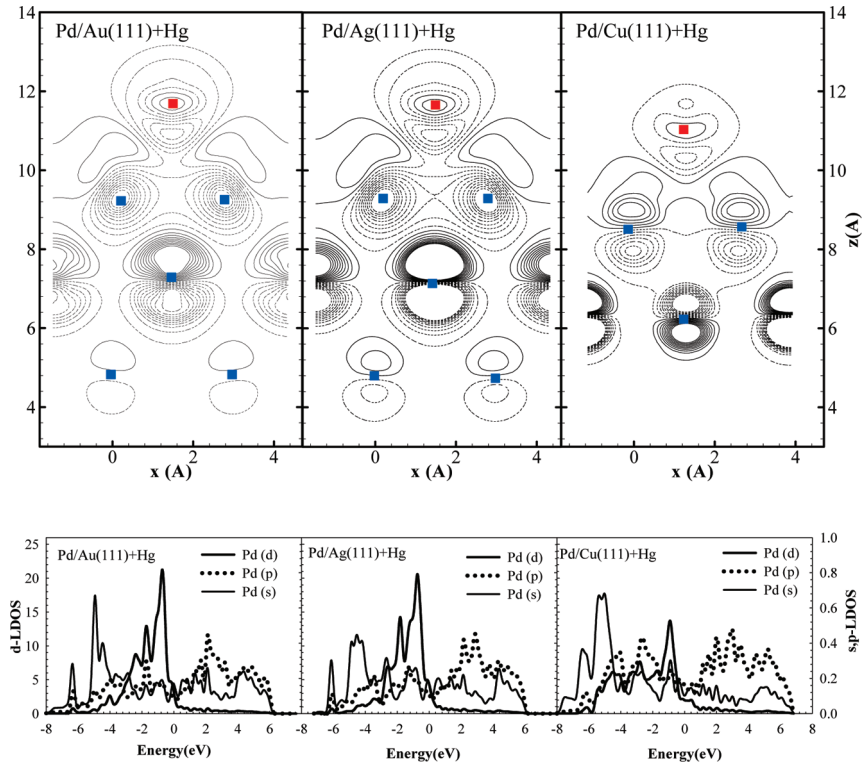

Figure 7. Charge density change on a Pd/M(111) surface along the direction normal and parallel to the surface and L-DOS graphs of surface Pd atoms after binding of Hg. In the top graphs, dashed lines repesent the negative charge transfer (accumulation of electrons), whereas solid lines represent the positive charge transfer (i.e., depletion of electrons). Red squares depict the Hg atom, whereas blue squares depict the surface, first, and second subsurface layers.

Au(111) and 2Pd/Ag(111) surfaces becomes narrower because of the hybridization of the d-states of the surface atoms with the second layer atoms. Also, the d-band centers of the surface atoms on Pd/Au(111) and 2Pd/Ag(111) are found to be higher in energy, which leads to enhanced reactivity compared to the clean Pd(111) surface. In all the surfaces presented, the d-band of Hg strongly overlaps with the s- and p-band of Pd at approximately 7 eV. It appears that the s- and p-states of Pd form new resonance peaks at the Hg d-band energy for the 2Pd/Ag(111) surface, whereas for other surfaces, the shape of the s- and p-states of Pd is modified after Hg binding. Furthermore, the L-DOS plots of the $Pd_3Cu(111)$ surface before and after Hg binding suggest that the s-, p-, and d-bands of Cu are not affected significantly from the adsorbate interaction, which implies that Pd is the primary surface atom responsible for improving the binding of Hg. The L-DOS plots of gas-phase Hg and the adsorbed Hg atoms, presented in Figure 6, also illustrate the strong interaction of Hg with the surface. The d-band of Hg shifts down in energy with the surface interaction, and both the s- and p-state broaden and become lower in energy. All of these findings show a higher reactivity of the Pd surface atoms to Hg. In addition, on the $Pd_3Cu(111)$ surface, the binding of Hg is not expected to be as strong as those on Pd/Au(111) and 2Pd/Ag(111) surfaces because of the low-lying s-, p-, and d-band of Hg relative to the Pd overlays.

The surface dipole layer change in charge density along the direction parallel and normal to the surface and L-DOS of one of the Pd overlays after Hg binding was examined, as shown in Figure 7. In both the Pd/Au(111) and Pd/Ag(111) graphs, it is possible to observe marked changes in the charge density of the surface, first subsurface, and second subsurface layers upon Hg binding due to the strong Hg interaction. The negative and positive values in charge density indicate accumulation and depletion of electrons, respectively. It is clear that electrons accumulate on surface layers in the case of Au and Ag hosts and subsequently affect the charge distribution in the subsurface layers. The solid lines located around the Hg atom indicate a charge transfer from Hg to the surface. A Bader charge analysis[64,65] of the charge density also demonstrates a charge transfer (−0.07e) from Hg to the surface atoms on the Pd/M(111) overlays, which is consistent with the change in work function. The charge density difference between the surface layer and adsorbate has positive values approximately 1 Å from the surface, indicating the depletion of electrons from these regions and their corresponding contribution to bonding. For the Pd/Cu(111) overlays, the charge density change is not as significant as Pd/Au(111) and Pd/Ag(111) overlays leading to an unchanged charge density in the second subsurface layer. Again, charge distribution is reorganized within the surface and first subsurface layers as a consequence of charge transfer from Hg to the surface atoms in Pd/Cu(111) overlays upon Hg binding. The L-DOS graphs of surface Pd atoms are also consistent with the charge transfer analysis. In comparison to the Cu host atoms, the d-bandwidth of the surface Pd atoms is found to be narrower on Au and Ag, which signifies the strong Hg interaction on Au and Ag hosts. Furthermore, s- and p-states of Pd overlap with the d-band of Hg, modifying the shape of the states at approximately 7 eV; however, in the case of Au and Ag hosts, these states showed narrower and sharper peaks at the same energy due to the strong Hg interaction.

Conclusions

The binding and electronic structures of Hg are investigated on Pd binary alloys and overlays. The binding of Hg is found to be dominated mostly by the Pd atoms located in the surface layers. Furthermore, the position of the M atoms located in both the surface and the subsurface layers may enhance and reduce

the reactivity of the surface, respectively. When Pd is deposited on the top of another metal having larger lattice spacing, the lattice constant of the overlaid substrate matches that of the underlying metal, resulting in an upshift in energy of the surface Pd atom d-states, leading to increased surface reactivity. In addition, there is an indirect interaction between Hg and the subsurface layer, when Au and Ag are present, which leads to an increase in the binding interaction. Analysis of the L-DOS of the surface atoms showed that there is a significant overlap between the s- and p-states of Pd and the d-states of Hg, leading to a strong adsorbate−substrate interaction. Lastly, a decrease in the work function with Hg binding indicates an electron transfer from Hg to the surface atoms.

The binding of S and Hg on Pd alloys is compared with each other, and both adsorbates are found to be attracted by the same surface adsorption sites studied in this work. It is important to note that in both gasification and combustion processes high S content might affect the reactivity of the metal surface and decrease its ability to capture Hg.

References and Notes

(1) Clarkson, T. W. *Environ. Health Perspect.* **1993**, *100*, 31.
(2) Energy Information Administration. Coal. http://www.eia.doe.gov/oiaf/ieo/pdf/coal.pdf (Accessed May 7, 2007).
(3) U.S. Environmental Protection Agency. Clean Air Mercury Rule. http://www.epa.gov/air/mercuryrule (accessed October 20, 2008).
(4) Granite, E. J.; Myers, C. R.; King, W. P.; Stanko, D. C.; Pennline, H. W. *Ind. Eng. Chem. Res.* **2006**, *45*, 4844.
(5) Poulston, S.; Granite, E. J.; Pennline, H. W.; Myers, C. R.; Stanko, D. C.; Hamilton, H.; Rowsell, L.; Ilkenhans, T.; Chu, W. *Fuel* **2007**, *86*, 2201.
(6) Steckel, J. A. *Phys. Rev. B* **2008**, *77*, 115412.
(7) Aboud, S.; Sasmaz, E.; Wilcox, J. *Main Group Chem.* **2008**, *7*, 205.
(8) Jones, R. G.; Tong, A. W. L. *Surf. Sci.* **1987**, *188*, 87.
(9) Singh, N. K.; Dale, P. A. D. M. A.; Bullett, D.; Jones, R. G. *Surf. Sci.* **1993**, *294*, 333.
(10) Soverna, S.; Dressler, R.; Düllmann, C. E.; Eichler, B.; Eichler, R.; Gäggeler, H. W.; Haenssler, F.; Niklaus, J. P.; Piguet, D.; Qin, Z. *Radiochim. Acta* **2005**, *93*, 1.
(11) Dowben, P. A.; Kime, Y. J.; Varma, S.; Onellion, M.; Erskine, J. L. *Phys. Rev. B* **1987**, *36*, 2519.
(12) Prince, N. P.; Singh, N. K.; Walter, W.; Woodruff, D. P.; Jones, R. G. *J. Phys.: Condens. Matter* **1989**, *1*, 21.
(13) Kime, Y. J.; Zhang, J.; Dowben, P. A. *Surf. Sci.* **1992**, *268*, 98.
(14) Poulsen, P. R.; Stensgaard, I.; Besenbacher, F. *Surf. Sci. Lett.* **1994**, *310*, L589.
(15) Singh, N. K.; Jones, R. G. *Surf. Sci.* **1990**, *232*, 229.
(16) Sarpe-Tudoran, C.; Fricke, B.; Anton, J.; Persina, V. *J. Chem. Phys.* **2007**, *126*, 174702.
(17) Eguchi, T.; Kamoshida, A.; Ono, M.; Hamada, M.; Shoda, R.; Nishio, T.; Harasawa, A.; Okuda, T.; Kinoshita, T.; Hasegawa, Y. *Phys. Rev. B* **2006**, *74*, 073403.
(18) El-Azizi, A. M.; Kibler, L. A. *J. Electroanal. Chem.* **2002**, *534*, 107.
(19) Kibler, L. A.; El-Aziz, A. M.; Hoyer, R.; Kolb, D. M. *Angew. Chem., Int. Ed.* **2005**, *44*, 2080.
(20) Lu, Y. F.; Przybylski, M.; Nývlt, M.; Winkelmann, A.; Yan, L.; Shi, Y.; Barthel, J.; Kirschner, J. *Phys. Rev. B* **2006**, *73*, 035429.
(21) Roudgar, A.; Gross, A. *J. Electroanal. Chem.* **2003**, *548*, 121.
(22) Roudgar, A.; Gross, A. *Phys. Rev. B* **2003**, *67*, 033409.
(23) Shao, M. H.; Huang, T.; Liu, P.; Zhang, J.; Sasaki, K.; Vukmirovic, M. B.; Adzic, R. R. *Langmuir* **2006**, *22*, 10409.
(24) Suzuki, T.; Hasegawa, Y.; Li, Z.-Q.; Ohno, K.; Kawazoe, Y.; Sakurai, T. *Phys. Rev. B* **2001**, *64*, 081403.
(25) Alfonso, D. R.; Cugini, A. V.; Sholl, D. S. *Surf. Sci.* **2003**, *546*, 12.
(26) Kresse, G.; Hafner, J. *Phys. Rev. B* **1993**, *48*, 13–115.
(27) Kresse, G.; Hafner, J. *Phys. Rev. B* **1994**, *49*, 14251.
(28) Kresse, G.; Furthmuller, J. *Comput. Mater. Sci.* **1996**, *6*, 15.
(29) Blöchl, P. E. *Phys. Rev. B* **1994**, *50*, 17953.
(30) Kresse, G.; Joubert, D. *Phys. Rev. B* **1999**, *59*, 1758.
(31) Perdew, J. P.; Chevary, J. A.; Vosko, S. H.; Jackson, K. A.; Pederson, M. R.; Singh, D. J.; Fiolhais, C. *Phys. Rev. B* **1992**, *46*, 6671.
(32) Wang, Y.; Perdew, J. P. *Phys. Rev. B* **1991**, *44*, 13298.
(33) Pearson, W. B. *Handbook of Lattice Spacings and Structures of Metals and Alloys*; Pergamon Press: New York, 1967; Vol. 2.
(34) Kittel, C. *Introduction to Solid State Physics*, 7th ed.; Wiley: New York, 1996.
(35) Monkhorst, H. J.; Pack, J. D. *Phys. Rev. B* **1976**, *13*, 5188.
(36) Muller, S.; Zunger, A. *Phys. Rev. Lett.* **2001**, *87*, 165502.
(37) Hultgren, R.; Desai, P. A.; Hawkins, D. T.; Gleiser, M.; Kelly, K. K. *Selected Values of the Thermodynamics Properties of Binary Alloys*; American Society for Metals: Metals Park, OH, 1973.
(38) Villars, P.; Calvet, L. D. *Pearson's Handbook of Crystallographic Data for Intermetallic Phases*; ASM International: Materials Park, OH, 1991.
(39) Kumar, D.; Chen, M. S.; Goodman, D. W. *Catal. Today* **2007**, *123*, 77.
(40) Lee, Y.-S.; Jeon, Y. *J. Korean Chem. Soc.* **2000**, *37*, 51.
(41) Wigner, E.; Bardeen, J. *Phys. Rev.* **1935**, *48*, 84.
(42) Leung, T. C.; Kao, C. L.; Su, W. S.; Feng, Y. J.; Chan, C. T. *Phys. Rev. B* **2003**, *68*, 195408.
(43) Gsell, M.; Jakob, P.; Menzel, D. *Science* **1998**, *280*, 717.
(44) Jakob, P.; Gsell, M.; Menzel, D. *J. Chem. Phys.* **2001**, *114*, 10075.
(45) Bligaard, T.; Norskov, J. K. *Electrochim. Acta* **2007**, *52*, 5512.
(46) Kibler, L. A.; Kleinert, M.; Randler, R.; Kolb, D. M. *Surf. Sci.* **1999**, *443*, 19.
(47) Hasegawa, Y.; Jia, Y. F.; Inoue, K.; Sakai, A.; Sakurai, T. *Surf. Sci.* **1997**, *386*, 328.
(48) Takahasi, M.; Hayashi, Y.; Mizuki, J.; Tamura, K.; Kondo, T.; Naohara, H.; Uosaki, K. *Surf. Sci.* **2000**, *46*, 213.
(49) Naohara, H.; Ye, S.; Uosaki, K. *J. Electroanal. Chem.* **2001**, *500*, 435.
(50) Quayum, M. E.; Ye, S.; Uosaki, K. *J. Eletroanal. Chem.* **2002**, *520*, 126.
(51) Paniago, P.; de Siervo, A.; Soares, E. E.; Pfannes, H.-D.; Landers, R. *Surf. Sci.* **2004**, *560*, 27.
(52) Wadayama, T.; Abe, K.; Osano, H. *Appl. Surf. Sci* **2006**, *253*, 2540.
(53) Christensen, A.; Ruban, V.; Stiolze, P.; Jacobsen, K. W.; Skriver, H. L.; Nørskov, J. K.; Besenbacher, F. *Phys. Rev. B* **1997**, *56*, 5822.
(54) Hammer, B.; Scheffler, M. *Phys. Rev. Lett.* **1995**, *74*, 3487.
(55) Hammer, B.; Nørskov, J. K. *Surf. Sci.* **1995**, *343*, 211.
(56) Hammer, B.; Morikawa, Y.; Nørskov, J. K. *Phys. Rev. Lett.* **1996**, *76*, 2141.
(57) Hammer, B.; Nielsen, O. H.; Nørskov, J. K. *Catal. Lett.* **1997**, *46*, 31.
(58) Ruban, A.; Hammer, B.; Stoltze, P.; Skriker, H. K.; Nørskov, J. K. *J. Mol. Catal. A: Chem.* **1997**, *115*, 421.
(59) Mavrikakis, M.; Hammer, B.; Nørskov, J. K. *Phys. Rev. Lett.* **1998**, *81*, 2819.
(60) Pallassana, V.; Neurock, M.; Hansen, L. B.; Hammer, B.; Nørskov, J. K. *Phys. Rev. B* **1999**, *60*, 6146.
(61) Hammer, B.; Nørskov, J. K. *Adv. Catal.* **2000**, *45*, 71.
(62) Liu, P.; Nørskov, J. K. *Phys. Chem* **2001**, *3*, 3814.
(63) Huger, E.; Osuch, K. *Europhys. Lett.* **2005**, *71*, 276.
(64) Bader, R. F. W. *Atoms in Molecules: A Quantum Theory*; Oxford University Press: New York, 1990.
(65) Henkelman, G.; Arnaldsson, A.; Jónsson, H. *Comput. Mater. Sci.* **2006**, *36*, 254.

JP8112478